Available online at www.sciencedirect.com
SCIENCE DIRECT
Polymer 46 (2005) 6380–6390
polymer
www.elsevier.com/locate/polymer

Crystalline and amorphous deformation of process-controlled cellulose-II fibres

K. Kong, S.J. Eichhorn*

Materials Science Centre, School of Materials, University of Manchester, Grosvenor Street, Manchester M1 7HS, UK

Received 25 January 2005; received in revised form 13 April 2005; accepted 13 April 2005
Available online 1 July 2005

Abstract

Raman spectroscopy has been used as a tool to monitor the microdeformation of a range of process-controlled fibres with different orientations. The mechanical properties of the fibres are shown to be related to the orientation parameter ($\langle \sin^2\theta \rangle$), and that by using the particular fibre spinning process (*N*-methylmorpholine *N*-oxide (NMMO)/cellulose), a plateau is reached, beyond which no improvements can be made. Clear shifts in the 1095 cm^{-1} Raman band towards a lower wavenumber are observed upon the application of external tensile deformation, which are thought to relate to the molecular deformation of the cellulose chain. It is found that relationships are determinable between the rate of band shift with respect to strain of the 1095 cm^{-1} Raman band and the orientation parameter. For the first time, a modified series model is related to the molecular deformation as revealed by Raman spectroscopy, and that the data for these fibres is consistent with a structure with a dominant amorphous fraction. Other high modulus cellulose fibres are shown to behave more like high performance polymer fibres such as poly(*p*-phenylene benzobisoxazole) (PBO) and poly(*p*-phenylene terephtalamide) (PPTA). The need, if high performance variants of these fibres are to be developed, to improve the microstructure of NMMO–cellulose fibres is discussed.

Keywords: Raman; Cellulose; Microdeformation

1. Introduction

Liquid crystalline cellulose is desired as a starting material for the production of commercial forms of spun fibre filaments [1]. This is because it is known that the liquid crystallinity infers a high degree of order to the cellulose and ultimately generates fibres with high mechanical properties [1]. It has long been known, since initial studies by Graenacher and Sallman [2], that cellulose will readily dissolve in a non-derivative form in amine oxides. Since this discovery, many workers have conducted investigations into using amine oxides for dissolving cellulose, a historical review of which has been conducted by Woodings [3]. A schematic diagram of the structure of *N*-methylmorpholine *N*-oxide (NMMO), a common solvent used in commercially in the presence of water for the production of regenerated cellulose fibres of this type is shown in Fig. 1. Due to the high polarity of the N–O bond, the oxygen of this group is able to form one or two hydrogen bonds with hydroxylated substances such as cellulose [4,5]. Liquid crystalline effects have also been observed with this system [6], not only in the spinning solution, but also during the spinning process. However, it is worth noting at this point that the mechanical properties obtained by various workers for fibres that produce mesophases and liquid crystallinity effects with non-derivitised cellulose in anisotropic phosphoric acid far exceed those obtainable by this route [7–9]. However, investigations of the structure and properties of NMMO-based fibres such as lyocell have been extensive. Studies by a number of workers (see Refs. [10–16] for some examples) have led to conclusion that these fibres consist of a cellulose-II structure, and are distinguished by high crystallinity, long crystallites, a high degree of orientation, and well-oriented amorphous regions. However, this is again not realised in the mechanical properties of such fibres. Relationships between the mechanical properties and structure of regenerated cellulose fibres derived from the NMMO–cellulose system have been studied recently. In particular, the high orientation and fibrillar nature of these

* Corresponding author. Tel.: +44 161 306 5982; fax: +44 161 306 3586.
E-mail address: s.j.eichhorn@manchester.ac.uk (S.J. Eichhorn).

0032-3861/$ - see front matter © 2005 Elsevier Ltd. All rights reserved.
doi:10.1016/j.polymer.2005.04.096

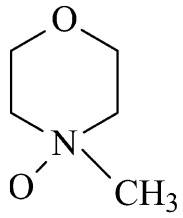

Fig. 1. Schematic structure of the NMMO (*N*-methylmorpholine *N*-oxide) solvent.

fibres has been investigated using peelback testing [17] where it was found that these properties give rise to the mechanical properties observed. X-ray diffraction has also been utilised to determine the orientation and long-periods of these fibres, after treatment with NaOH, relating their evolution of structure to mechanical properties [18].

Raman spectroscopy, as a tool for understanding the deformation micromechanics of polymeric fibres (and other materials), has gained increasing interest in recent times. The principle relies on monitoring the shift towards a lower wavenumber of a Raman band that is characteristic of the molecular backbone of the polymer, upon the application of tensile deformation. Shifts of this type have been shown to be indicative of direct molecular deformation [19] and can be used as a tool to understand the mechanics of polymer fibres [20]. Using this method, conventional man-made polymeric fibres have been studied [20] and more recently a number of regenerated cellulose fibres from a number of sources have also been investigated [21–23]. The molecular deformation process, and the shift in the 1095 cm^{-1} Raman band for cellulose has also recently been modeled for high performance regenerated cellulose fibres [24]. In this study, we report on the molecular deformation of comparatively lower modulus regenerated cellulose fibres, as determined by Raman spectroscopy. The molecular deformation is shown to directly relate to the orientation of the structure, and it is shown that although molecular orientation plays a key role in the fibre mechanics, other factors such as hydrogen bonding void structure and in particular, the amorphous fraction may also be critical. In this respect, Raman spectroscopy if shown to be useful for relating the local fibre micromechanics directly to the mechanical properties of cellulose fibres, and that structural information can be ascertained from this.

2. Experimental methods

2.1. Materials

The materials used in this study were single filaments of experimentally spun cellulose fibres. All fibres were generated using a NMMO (*N*-methlymorpholine *N*-oxide) solvent with wood-pulp as the source of cellulose. The spinning 'dopes' contained 14% cellulose and 86% NMMO.

2.2. Fibre spinning

Pilot-scale fibre spinning equipment (supplied by ACORDIS-Tencel (now Lenzing)) was used to produce fibres by wet-jet spinning. The spinning 'dope' was then placed into a spinnaret and extruded at a temperature of 95 °C through an air gap into a coagulation bath. The spinnaret dopes were extruded using controlled speeds, and cooled with a jet of air across the filament. The coagulant used in the spinning bath was water, which is known to solvent exchange with the NMMO, and induce hydrogen bonding [5]. All fibres produced by this method were wound in a continuous filament using a controlled speed onto a rotating drum, and then washed with water and dried at room temperature. A number of draw ratios (take-up speed/dope speed) were used to produce these fibres; namely 8.9, 5.9, 2.9, 1.5, 1.1, and 0.7.

Prior to obtaining other physical properties, diameters of single filaments of all samples (commercial and experimentally spun) were determined. This was done using a calibrated Phillips 525M field emission gun (FEG), scanning electron microscope (SEM). Samples were placed in the evacuated chamber of the SEM on an electrically conductive stub. The fibres were secured to the stub using carbon paper, and were also carbon coated. The samples were scanned using an accelerating voltage of 5 kV and images were taken along the fibre lengths. These images were then processed using image analysis software, and assuming a circular cross-section for the filaments, 30 measurements of the diameters of each fibre sample were used to obtain a mean cross-sectional area.

2.3. Birefringence and orientation of fibres

The method used to obtain the fibre birefringence using a Berek compensator, and ultimately the orientation, is one that has been described more completely by Morton and Hearle [25]. Single fibre samples were observed using an Olympus BH-2 optical microscope and a monochromatic light source (589.6 nm). Linear polarised light passing through the fibre was further retarded using a Berek compensator, and two linear polarisers were placed perpendicular to each other and rotated at 45° to the fibre axis. The fibres were prepared on a thin glass slide before measurements were taken. The image of the fibre appears dark when the sum of the retardation of the Berek compensator and the fibre is zero. Hence, the birefringence (Δn) of the fibre can be obtained simply from the compensator crystal tilt angle (ϕ) and the fibre diameter (d). The latter was determined optically directly from images obtained on the microscope, and the birefringence was obtained using the equation [26]

$$\Delta n = \frac{R(\phi)}{d} \tag{1}$$

where $R(\phi)$ is the retardation as a function of tilt angle,

which was obtained empirically by using a standard calibration procedure. Assuming that the high degree of orientation in the fibre gives rise to the birefringent effects observed, and not as a result of 'form birefringence' [27], this method was used to obtain values for all fibres.

To obtain the orientation parameter $\langle \sin^2\theta \rangle$ for the fibres, an analysis first suggested by Hermans [28] was used. The expression used to obtain the orientation parameter from the birefringence is given as [28]

$$\frac{\Delta n}{\Delta n_{\max}} = 1 - \tfrac{3}{2}\langle \sin^2\theta \rangle \quad (2)$$

where $\Delta n_{\max}$ is the maximum birefringence, the value of which can easily be determined graphically.

2.4. Mechanical properties of fibres

Single filaments for all fibre samples were secured using cold-curing epoxy resin (supplied by Ciba-Geigy) to fibre testing cards prior to deforming in tension. A number of gauge lengths were used (5, 10, 30, 50, 80 and 100 mm) for the tests to extrapolate to true breaking strengths and moduli. After the fibres had been mounted into the jaws of an Instron-1121 universal testing machine, with a 1 N load cell, the sides of the fibre testing card were burnt away using an artist's pyrography machine. The cross-head speed during fibre deformation was set at a strain rate of 0.166% s^{-1}. For each gauge length, 20 samples were tested for statistical reliability. All samples were deformed under controlled conditions of temperature (23 ± 1 °C) and humidity (50 ± 5%). Young's moduli of the fibres were determined, as the slope to the initial portion of the stress–strain curve, as well as the ultimate breaking strengths and strains.

2.5. Micromechanical properties of fibres using Raman spectroscopy

A Renishaw system 1000 Raman spectrometer was used to determine the micromechanics of single fibre filaments during tensile deformation. Samples, secured to fibre testing cards as described in the previous section, were deformed on a customised loading rig with a 1 N load cell and a micrometer to record macroscopic deformation parameters. This loading rig was placed onto the stage of an Olympus microscope, which is coupled to the main Raman spectrometer unit. A He–Ne laser (25 mW, 632.8 nm) was used to irradiate the fibres, and obtain the Raman spectra, and this was focussed to a spot size of about 2 μm on the surface of the samples using a ×50 lens. Raman spectra were taken using an exposure time of 240 s to ensure clarity for peak fitting purposes. After each spectrum was obtained, the samples were deformed in tension using strain increments of 0.5%. Spectra were obtained in the range 1050–1150 cm^{-1}, since the position of the 1095 cm^{-1} Raman band was of particular interest to this study. This band has been shown previously to shift towards a lower wavenumber upon the application of tensile deformation [9,19,20] and hence was considered to be a reliable indicator of molecular deformation. All spectra were recorded using a highly sensitive, Peltier-cooled charged coupled device, which was connected to a PC interface. To obtain the central position of the 1095 cm^{-1} Raman peak, all spectra were fitted using a Lorentzian function, based on an algorithm developed by Marquardt [29].

3. Results and discussion

3.1. Fibre spinning and effect on diameter

The diameters of the fibres decreased non-linearly with increasing draw ratio as can be seen in Fig. 2. The fit to the data is from a model suggested by Mortimer and Péguy [30] that assumes a conservation of volumetric flow rate, and gives a theoretical prediction of fibre diameter (d) as function of draw ratio (D_R) as

$$d = (D_R)^{-a} d_0 \quad (3)$$

where d_0 is the spinneret diameter and a is given a value of 0.50. The model fit to the data in this study, given that d_0 is 33 μm, gave a value of a of 0.48 which is of the same order as that determined by Mortimer and Péguy [30]. It is clear, however, from the data that there is a limit to the diameter of fibres obtainable by this spinning method. Also noticeable is a larger standard deviation in diameter for the smallest draw ratio ($D_R = 0.74$). This is because when the draw ratio becomes less than unity a die swell effect becomes significant at the spinneret which causes small fluctuations in the fibre diameter, and hence the standard deviation of the fibres from this experimental run are more variable in diameter.

All fibre samples were examined under the Scanning Electron Microscope, as already described, and the results of this analysis are summarised in Table 1.

3.2. Birefringence and orientation of fibres

The effect of the draw ratio on the birefringence, and hence the orientation parameter of the fibres, is shown in

Table 1
The effect of draw ratio (D_R) on the fibre diameter for a range of experimentally spun cellulose filaments

Draw ratio, D_R	Mean fibre diameter (μm)
8.9	11.2±0.7
5.9	13.8±0.6
2.9	19.5±0.5
1.5	26.7±0.8
1.1	33.0±0.7
0.7	37.7±2.0

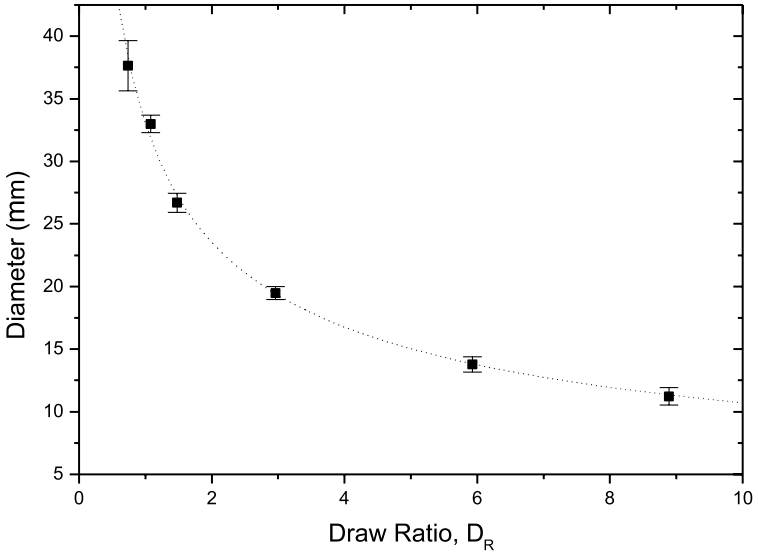

Fig. 2. The fibre diameter as a function of draw ratio (D_R).

Fig. 3. The birefringence is seen to increase with increasing draw ratio, an effect that one would expect since the anisotropy of the refractive indices parallel and perpendicular to the drawing direction is likely to increase under these circumstances. There will also therefore be a decrease in the orientation parameter with increasing draw ratio, with a smaller value indicating a higher orientation of the cellulose polymeric chains within the fibre. However, it is clear that there is a plateau in the maximum birefringence, and consequently the minimum orientation parameter, which further indicates that there is a limit to the orientation that one can achieve using this process. This limitation may be due to the effect of amorphous domains of cellulose chains limiting and constraining further orientation of crystalline regions, but remains a possibility and a subject for further investigation.

3.3. Mechanical properties of fibres

Typical stress–strain curves for fibres produced using different draw ratios are shown in Fig. 4. All curves indicate characteristically non-linear stress–strain behaviour [25] with an initial linear region up to about 1% strain. At 1% there is a yield-point, with a subsequent strain-hardening region to the curve. As can be seen from Fig. 4 the initial stiffness, or Young's modulus, and the slope of the strain hardening regions of the fibre's stress–strain curves increases with increasing draw ratio. This is thought to be due to the fact that by increasing the draw ratio, the molecular chains of cellulose become more oriented, and hence the stiffness of the material increases. This concept is substantiated by the increase in birefrigence as previously reported (cf. Fig. 3). If one plots the modulus of the fibres

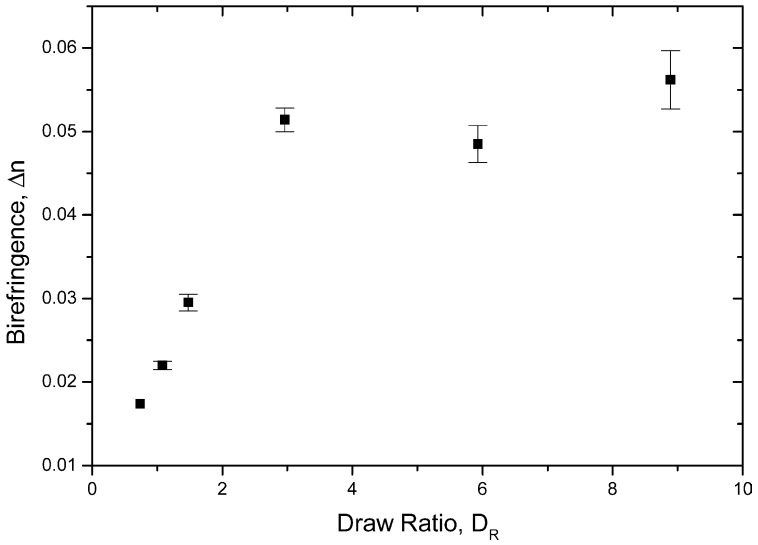

Fig. 3. The fibre birefringence as a function of draw ratio (D_R).

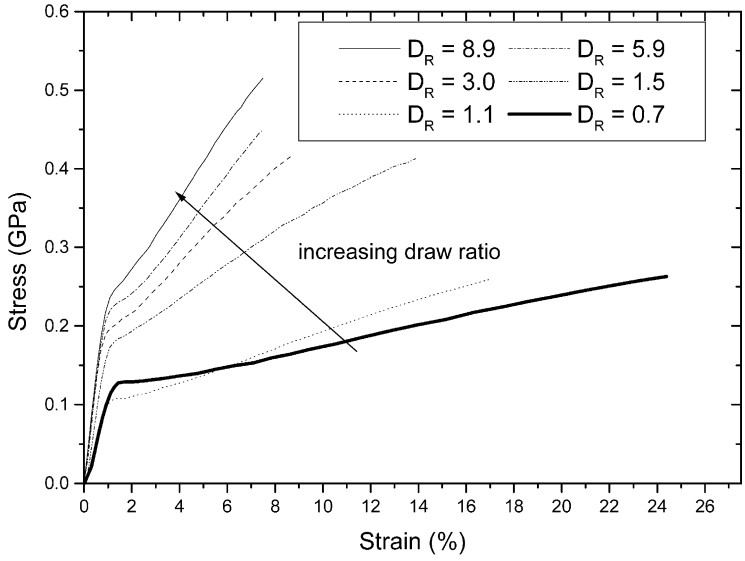

Fig. 4. The stress–strain curves for all experimentally spun cellulose fibres for a number of draw ratios (D_R = 8.9, 5.9, 3.0, 1.5, 1.1, 0.7).

against the orientation parameter ($\langle \sin^2\theta \rangle$), which is related to birefringence by Eq. (2), then one finds that this relationship is generally true, and this will be discussed later on. However, a summary of all mechanical properties is given in Table 2. The values for the breaking strength and the Young's modulus are from the extrapolation to a zero and an infinite gauge length, respectively.

3.4. Micromechanical properties of fibres using Raman spectroscopy

Typical Raman spectra obtained for the experimentally spun fibres (at two different draw ratios, D_R = 8.9 and 0.7) in the region between 500 and 3000 cm^{-1} are shown in Fig. 5(a). Both spectra have a similar profile, since each is thought to have a cellulose-II type structure [31]. The vast majority of assignments of the Raman bands for cellulose-II have been made by Wiley and Atalla [32]. In particular they assigned the dominant 1095 cm^{-1} Raman band highlighted in Fig. 5(a) to represent the stretch of C–O ring modes, although others [33] have assigned this to the glycosidic ring stretch (C–O–C). The position of this band has previously been shown to be sensitive to the application of external deformation on cellulose-II fibres from a variety of sources [9,21–23]. This was also found to be the case with the samples investigated here, and a typical shift in the 1095 cm^{-1} Raman band towards a lower wavenumber upon the application of tensile deformation is shown in Fig. 5(b). This shift is thought to be due to direct molecular deformation of the cellulose chains, as has been discussed before [9,21–23]. The 1095 cm^{-1} band shift shown in Fig. 5(b) is also characterised by an asymmetric broadening of the peak, and this will be discussed further in more detail later on. However, the effect of a controlled increase in orientation on the microdeformation of cellulose-II fibres has not previously been reported. In Fig. 6(a), typical Raman band shifts are reported in the peak positions of the 1095 cm^{-1} band as a function of strain, along with the shifts with applied stress in Fig. 6(b). Fig. 6(a) shows that as the draw ratio increases there is an increase in the Raman band shift rate. This is expected since the orientation of the fibres will increase with increasing draw ratio, and hence the deformation along the chain will increase therefore yielding a greater Raman band shift rate. A summary of all the band shift rates with respect to strain and stress is reported in Table 3. It can be seen that the highest draw ratio fibre (D_R = 8.9) has a strain band shift rate of 0.43 cm^{-1}/% which compares to values previously obtained for high

Table 2
The effect of draw ratio (D_R) on the fibre modulus (E), the breaking strength (σ_f) and the breaking strain (ε_f) for a range of experimentally spun cellulose filaments

Draw ratio, D_R	E (GPa)	σ_f (GPa)	ε_f (%)
8.9	26.0±0.6	0.559±0.011	9.0±0.3
5.9	23.0±0.5	0.522±0.013	10.2±0.5
3.0	19.0±0.7	0.427±0.010	11.1±0.4
1.5	14.5±0.5	0.319±0.009	16.0±0.6
1.1	13.2±0.5	0.300±0.007	18.3±1.1
0.7	11.2±0.2	0.274±0.002	27.8±1.0

Table 3
The effect of draw ratio (D_R) on the Raman strain band shift rate ($d\nu/d\varepsilon$) and the stress band shift rate ($d\nu/d\sigma$) for a range of experimentally spun cellulose filaments

Draw ratio, D_R	$d\nu/d\varepsilon$ (cm^{-1}/%)	$d\nu/d\sigma$ (cm^{-1}/GPa)
8.9	0.43±0.02	4.46±0.26
5.9	0.40±0.05	5.66±0.64
3.0	0.38±0.05	4.08±0.45
1.5	0.28±0.02	5.12±0.55
1.1	0.25±0.02	5.06±0.87
0.7	0.16±0.02	6.34±1.08

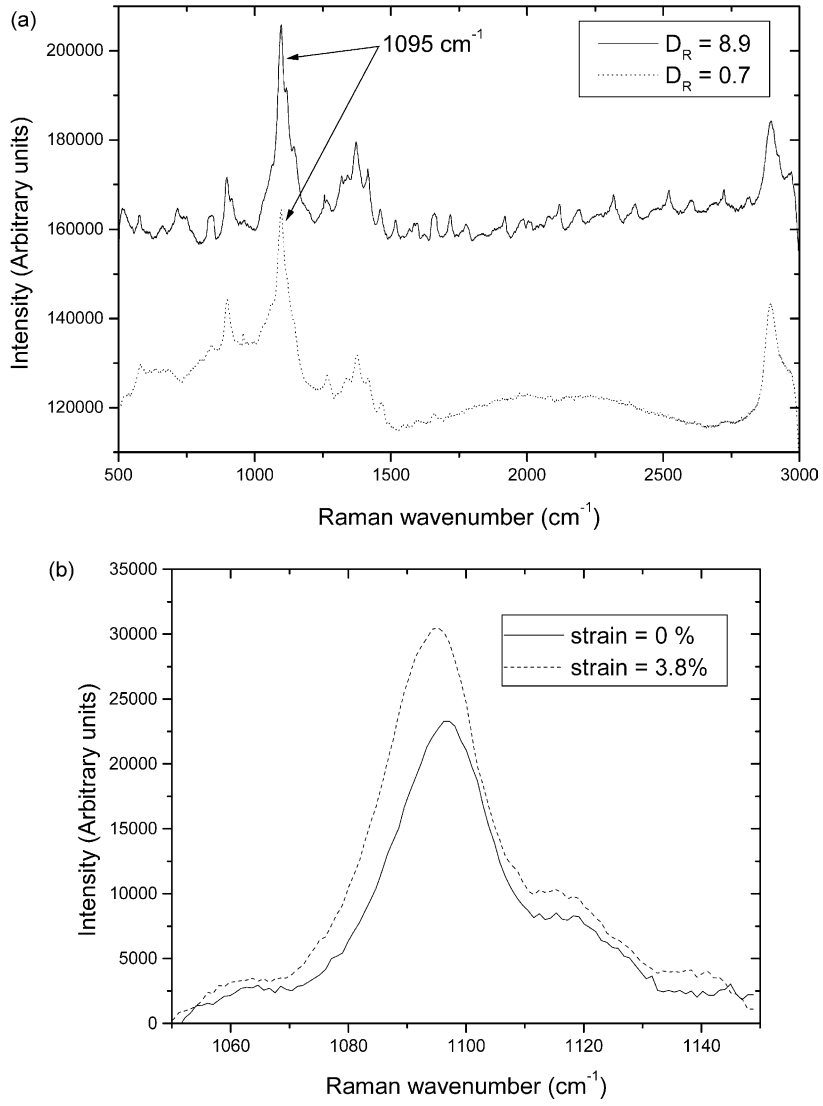

Fig. 5. The Raman spectra (a) for two experimentally spun cellulose fibres (D_R = 8.9 and 0.7) highlighting the position of the 1095 cm^{-1} peak and (b) for the position of the 1095 cm^{-1} peak as a function of tensile strain.

modulus Cordenka fibres [23] of between 0.7 and 0.9 cm^{-1}/% and a high modulus cellulose fibre produced by a liquid crystalline process [9] of 1.08 cm^{-1}/%. The shift rate with respect to strain is clearly not as high for a high performance cellulose fibre, but higher than that obtained [9] for a low modulus viscose fibre (0.1 cm^{-1}/%). Since the shift rate with respect to strain for cellulose is an indication of the transfer of external deformation to the direct straining of the polymeric backbone of the structure, then one can see that this process is not as dominant in these fibres. This will be discussed in more depth later on. However, the stress band shift rates can be seen to be comparable, irrespective of draw ratio applied to the fibre (at about 5 cm^{-1}/GPa) which is consistent with the findings of a previous study [23]. However, as one can see from Table 3, at low draw ratios the stress band shift rate has a large error associated with it. This is because of the increased non-linearity in the shift versus stress profile (cf. Fig. 6(b)), due to time-dependant effects, and a possible effect of low orientation. With fibres produced using draw ratios of less than unity, it was found that stress relaxation occurred to a much greater extent, and this is thought to be due to the misoriented chains acting rather like a spring to restore the applied stress. An increase in the Raman band shift rate with strain, as a function of the draw ratio, can be seen in Fig. 6(c). It is clear that there is a limit to the molecular deformation in these particular cellulose-based fibres, and this will therefore have implications for their ultimate tensile properties.

3.5. Theoretical approach to fibre micromechanics

An analysis derived by Northolt [34] and Northolt et al. [35] has been used to relate the modulus of a highly oriented polymeric fibre (E) to the crystal modulus (e_k) by the relationship

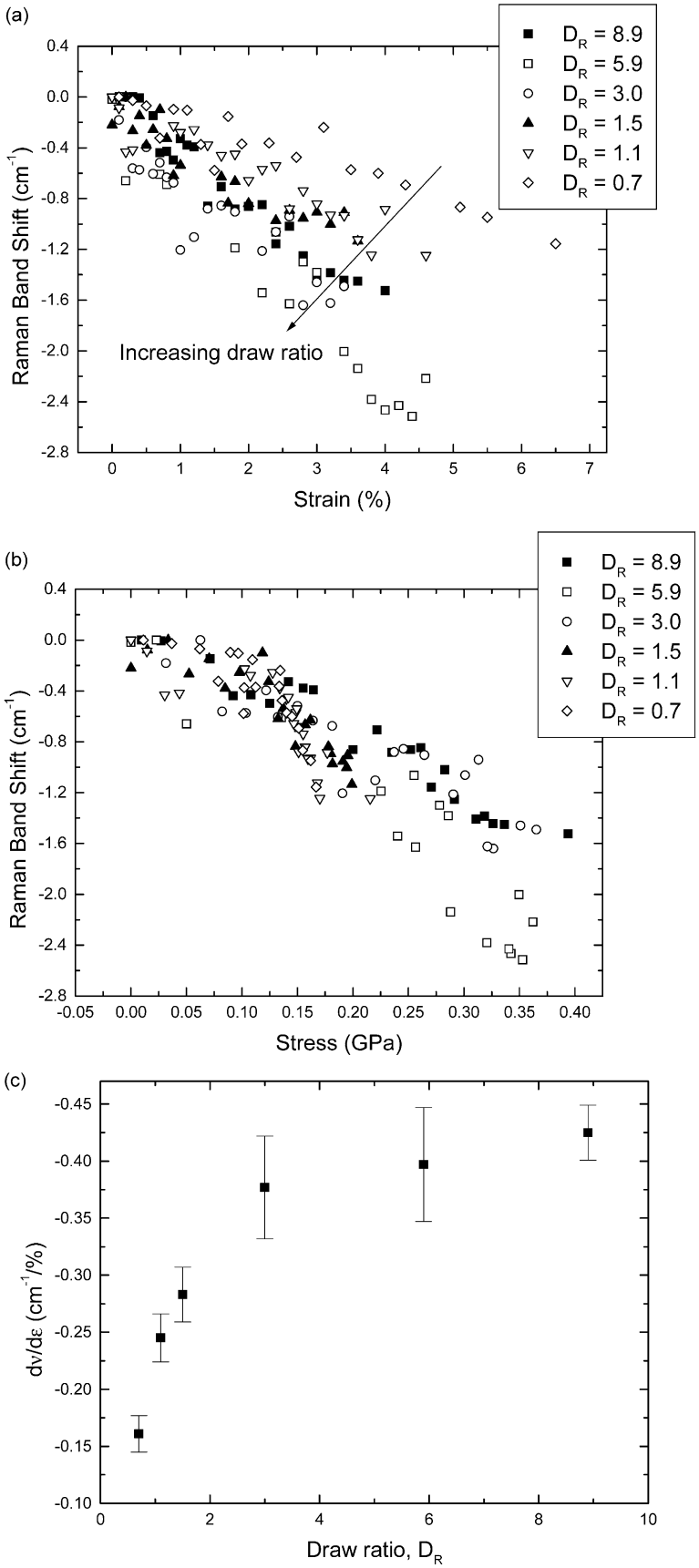

Fig. 6. The Raman band shifts in the central position of the 1095 cm^{-1} peak for all experimentally spun fibres with a number of draw ratios (D_R = 8.9, 5.9, 3.0, 1.5, 1.1, 0.7) with respect to (a) strain, (b) stress and (c) the shift rate with respect to strain ($d\nu/d\varepsilon$) as a function of draw ratio (D_R).

$$\frac{1}{E} = \frac{1}{e_k} + \frac{\langle \sin^2\Theta \rangle_E}{2g} \tag{4}$$

where $\langle \sin^2\Theta \rangle_E$ is the second moment of the orientation parameter (at zero load) and g is the shear modulus. The parameter $\langle \sin^2\Theta \rangle$ differs slightly from the definition of the orientation parameter used in Eq. (2) ($\langle \sin^2\theta \rangle$) but this shall be ignored for the sake of this analysis.

In a study by Northolt and de Vries [36] on the mechanical properties of regenerated and native cellulose fibres, a relationship is derived from Eqs. (4) and (2) to obtain the expression

$$\Delta n = \Delta n_{\max}\left(1 + \frac{3g}{e_k}\right) - \frac{3g\Delta n_{\max}}{E} \tag{5}$$

where $\Delta n_{\max}$ is the maximum orientation of a perfectly aligned fibre and g is the shear modulus of the fibre. Furthermore, they state that in a plot of Δn against $1/E$ the slope and the intercept (on the Δn axis, corresponding to a perfectly oriented fibre, i.e. $\Delta n_{\max}$) are related by the equation [8]

$$\frac{\text{slope}}{\text{intercept}} = \frac{3g}{1 + (3g/e_k)} \tag{6}$$

This type of analysis has been performed on the data from these experimentally spun fibres, the result of which is shown in Fig. 7. It shows that there is a linear relationship between Δn and the reciprocal modulus, and a value of 0.081 for $\Delta n_{\max}$ is obtained. Two literature values of this parameter ($\Delta n_{\max}$) can be found; one by Bingham [37] and another by Lenz et al. [14] of 0.056 and 0.061, respectively. Hence, by using this method, a higher value of this parameter has been obtained. One obtains a value of 3.6 GPa for the shear modulus (g) from Eq. (6), using a value of 98 GPa for e_k obtained recently by Eichhorn et al. [24] for a fully oriented cellulose-II chain. This value is a little higher than a value obtained (2.5 GPa) for a number of high modulus cellulose fibres by Northolt and deVries [36], and in the range of values obtained ($2.4 \leq g \leq 3.8$ GPa) for a liquid crystalline cellulose fibre (fibre B) [8,9]. It is, however, of the same order as obtained for a poly(*p*-phenylene terephthalamide) fibre, which is surprising given its much lower modulus [35]. The maximum modulus of these fibres (26.0 ± 0.6 GPa, cf. Table 2) is almost half that obtained for a high modulus cellulose-II fibre spun from a liquid crystalline solution (41.7 ± 0.2 GPa)[1]. High shear between crystalline domains would usually give rise to a high fibre modulus. Since the shear modulus (or shear parameter as it is sometimes called) is clearly of the same order of magnitude as other high performance fibres, including cellulose-derived materials, there must be other factors that determine that this fibre should have a relatively

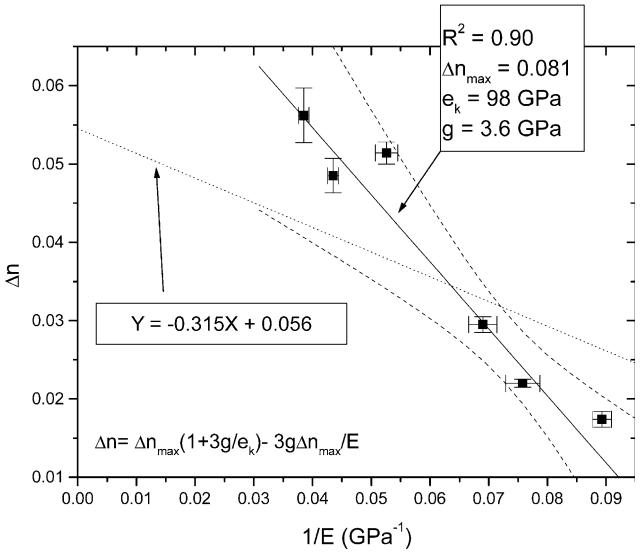

Fig. 7. The change in fibre birefringence (Δn) as a function of the reciprocal fibre modulus ($1/E$) showing two fits to the data using the equation $\Delta n = \Delta n_{\max}(1+3g/e_k) - 3g\Delta n_{\max}/E$ and values of $\Delta n_{\max} = 0.081$, $e_k = 98$ GPa and $g = 3.6$ (solid line; two dashed lines correspond to the 95% confidence bands) and for a value of $\Delta n_{\max} = 0.056$ showing the fitted equation values (dotted line).

small modulus. Skin-core structures have been observed within these types of fibres using small angle X-ray scattering [38], where the core of the fibres was found to contain larger and less oriented voids than the skin. Although no wide-angle data on the orientation of crystalline domains in the material has been reported, it does suggest that there may be a profile of orientation across the fibre, which has been previously postulated to reduce the modulus of regenerated cellulose fibres [24]. However, it is also pertinent to note the observations made by Northolt and De Vries [36] on the hydrogen bond system in cellulose-II structures. They state that the reason why cellulose-I fibres generally have higher moduli than cellulose-II derived structures is because of the mixture of single and double intramolecular hydrogen bonding between the anhydroglucose units. The hydrogen bonding system in cellulose-II has recently been revised for mercerised cellulose [39,40] and by another study using vibrational spectroscopic techniques [41]. Both studies indicate a 3D network of hydrogen bonds within the structure, and although in technical detail differ from the models previously proposed for cellulose-II hydrogen bond systems in relation to modulus [42], still have one intramolecular hydrogen bond per repeat unit (cellobiose) compared to cellulose-I. However, all these recent studies have focussed on mercerised cellulose [39–42], and this structure may differ in its hydrogen bonding to cellulose-II derived by dissolution. Early studies of this form of cellulose-II have tended to focus on derivitised cellulose, and not liquid crystalline solutions. It therefore appears apposite to study the differences between these two structures, and the chain stiffnesses, and this will be a topic for future publications. The liquid crystalline fibre (fibre B)

[1] Northolt et al. [8] quote a value of 58 GPa by a sonic method for the same fibre type.

that has been previously studied [7–9,24] appears to have a much higher modulus than other cellulose-II fibres, and this may be due to it retaining some of the hydrogen bond network of a cellulose-I structure.

If, alternatively, a plot of $1/E$ against the orientation parameter ($\langle\sin^2\theta\rangle$) for the fibres is performed, then one can obtain values for the shear parameter (g) and the crystalline modulus (e_k) using different values of the maximum birefringence. These plots are shown in Fig. 8(a) and (b) for two values of the maximum birefringence (Δn_{max} = 0.056 and 0.081). In this case, it is rather obvious that the crystal modulus obtained is sensitive to the value of the maximum birefringence used (25 and 135 GPa for Δn_{max} = 0.056 and 0.081, respectively). The shear parameters for each of these situations were found to be 4.9 and 3.3 GPa for Δn_{max} = 0.056 and 0.081, respectively. It is, therefore, clear that a reasonable estimate of maximum birefringence must first be obtained if reasonable values of the shear parameter and crystal modulus are to be obtained by this method.

However, let us now turn to the molecular deformation

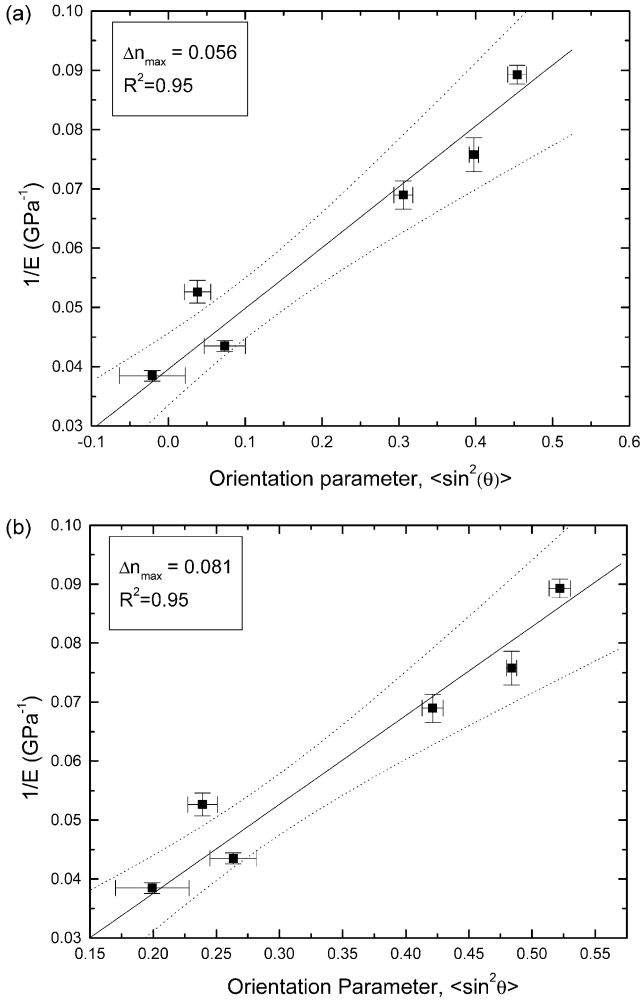

Fig. 8. The effect of orientation parameter ($\langle\sin^2\theta\rangle$) on the reciprocal of fibre modulus ($1/E$) for values of the maximum birefrigence (Δn_{max}) of (a) 0.056 and (b) 0.081.

information as revealed by the Raman method. If one assumes that the series model is correct, as has been assumed before for the modeling of a number of regenerated cellulose fibres [9,21–24], then one can relate the strain band shift rate ($d\nu/d\varepsilon$) to the stress band shift rate ($d\nu/d\sigma$) via the relationship

$$\frac{d\nu}{d\varepsilon} = \frac{d\nu}{d\sigma}\frac{d\sigma}{d\varepsilon} \tag{7}$$

Since the relationship $d\sigma/d\varepsilon$ is simply the modulus (E) of the series construction (cf. Eq. (4)) then one can write, taking k_σ to represent the stress band shift rate

$$\frac{d\nu}{d\varepsilon} = k_\sigma \frac{2e_k g}{2g + e_k\langle\sin^2\Theta\rangle} \tag{8}$$

By assuming, as before, that $\langle\sin^2\theta\rangle$ can be used as a reasonable estimate of $\langle\sin^2\Theta\rangle$, and that k_σ is a constant for a particular fibre type (assumed to be 4.5 cm^{-1}/GPa as found for the highest draw ratio fibre in this study (cf. Table 3)), then a plot of the strain band shift rate against the orientation parameter ought to follow the relationship given by Eq. (8). The experimental data, along with model fits of Eq. (8) using a variety of parameters are shown in Fig. 9, and as can be seen, they lie somewhat away from the lines predicted by Eq. (8). However, it is worth noting at this point that this equation is derived with the assumption that the material is fully crystalline [34,35]. If one assumes there is amorphous material in series with the crystals, with a reported [43] value of crystallinity (χ) of about 0.8, and that the modulus of the amorphous regions (e_a) is about 5 GPa, one can plot a similar curve with a reduced modulus according to the equation

$$\frac{d\nu}{d\varepsilon} = k_\sigma \frac{2e_k g e_a}{\chi e_a(2g + e_k\langle\sin^2\theta\rangle) + 2e_k g(1-\chi)} \tag{9}$$

This function has also been reported in Fig. 9 (solid bold line), for a crystal modulus of 98 GPa and a shear parameter of 3.5 GPa, and one can see there is better agreement, although not complete, with the data. More complex models could be derived, in a similar fashion to what has been done previously by Takayanagi et al. [44,45] where there is a parallel component of amorphous material (parallel-series construction [44,45]). This model could be favored from the point-of-view that in Fig. 5(b) asymmetric broadening of the 1095 cm^{-1} peak with tensile deformation was observed, which has been reported [24] to be an indication of this type of structure, wherein the crystals become overstressed during deformation. However, caution must be taken in this case, since the more parameters one introduces, the easier it becomes to fit the data and therefore the model can become more phenomenological, rather than based on any structural aspects of the polymer. In Fig. 9, the data for a crystalline, high modulus fibre (fibre B) from a previous publication [9] and a low modulus viscose fibre are also plotted for comparison. It is clear that the high modulus fibre falls on the line predicted for a fully series model of misoriented

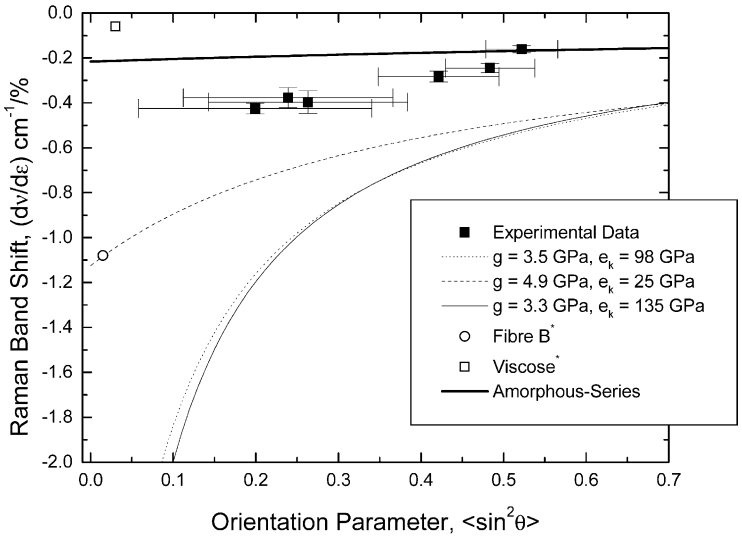

Fig. 9. The Raman band shift rate with respect to strain ($d\nu/d\varepsilon$) as a function of the orientation parameter ($\langle \sin^2\theta \rangle$) for all experimental fibres compared to values obtained for fibre B and viscose [9]. The lines shown are for the series aggregate model and for the amorphous series model, respectively.

crystalline domains [34,35], as used to explain the deformation of high performance, non-cellulosic fibres, such as PPTA and PBO [46]. This suggests that these high modulus cellulose fibres behave mechanically, because of their microstructure, in a similar fashion to other high performance polymeric fibres, and more importantly, clearly distinctive from other cellulose-II fibres. The low modulus viscose fibre (which has been reported [9] to have a modulus of about 9 GPa) is also plotted in Fig. 9, and the data point for this fibre is somewhat further from the lines predicted by Eq. (8) giving further evidence that these lower modulus possibly have very different structures, with more dominant amorphous regions, than fibre B.

The presence of amorphous regions in either in series and/or parallel to crystalline fractions of cellulose will have an effect on the local strain in the structure. If in parallel, the stress in each component (crystalline and amorphous) will be the same, according to the series aggregate model [34,35, 45]. However, since the Raman band shift is governed by the applied stress [20], the lower the magnitude of the Raman band shift itself will be in a polymeric fibre with a significant amorphous fraction. This, coupled with chain misorientation, which itself will give rise to an additional strain component, will locally yield a low strain/band shift rate. In the case where there is a parallel fraction of amorphous cellulose, both the strain and stress-transfer to the crystals will be governed by this fraction, and consequently the microdeformation revealed by Raman spectroscopy.

4. Conclusions

In conclusion then it has been shown that Raman spectroscopy is a powerful tool for understanding the deformation mechanisms in cellulose fibres produced using the NMMO–solvent system. Although liquid crystalline effects have been observed for this system, and high crystallinity and orientation also, these properties are not realised in the mechanics of the fibres compared to high performance cellulose fibres derived in recent times. It has been seen that clear shifts in the 1095 cm^{-1} Raman bands reveal a structure that may be a hybrid of a series aggregate model with significant amorphous fractions either in parallel and/or series with the misoriented crystals. Using theoretical models for the structure, and mechanics, it has been found that although the shear parameter for these fibres is as high as has been found for other high performance fibres (cellulosic and non-cellulosic), the modulus of the fibres still remains relatively low, and plateaus even if the draw ratio is increased. This suggests that further improvements must be made in the processing of these types of fibres. The NMMO/cellulose process is desirable since it has been reported [3] to be environmentally friendly compared to the viscose and certainly the liquid crystalline/phosphoric acid process reported recently [7,8].

Acknowledgements

The authors wish to thank Dr Roger Ibbett and Acordis-Tencel (now Lenzing) for valuable discussions and for the use of their pilot-plant fibre spinning equipment. This work was completed using funding obtained from the EPSRC (Grant No. EP/S44471/01).

References

[1] Northolt MG, Sikkema DJ. Adv Polym Sci 1991;98:115–77.
[2] Graenacher C, Sallmann R. US Patent Office 2179181; 1939.

[3] Woodings CR. Int J Biol Macromol 1995;17:305–9.
[4] Maia E, Péguy A, Pérez S. Acta Cryst 1981;37:1858–62.
[5] Chanzy H, Nawrot S, Peguy A, Smith P, Chevalier J. J Polym Sci B 1982;20:1909–24.
[6] Laszkiewicz B. Mol Cryst Liq Cryst 2000;353:127–31.
[7] Boerstoel H, Maatman H, Westerink JB, Koenders BM. Polymer 2001;42:7371–9.
[8] Northolt MG, Boerstoel H, Maatman H, Huisman R, Veurink J, Elzerman H. Polymer 2001;42(19):8249–64.
[9] Eichhorn SJ, Young RJ, Davies RJ, Riekel C. Polymer 2003;44: 5901–8.
[10] Lenz J, Schurz J, Wrentschur E. Holzforschung 1988;42:117–22.
[11] Lenz J, Schurz J, Wrentschur E. J Appl Polym Sci 1988;35: 1987–2000.
[12] Lenz J, Schurz J. Cell Chem Technol 1990;24:3–21.
[13] Lenz J, Schurz J. Cell Chem Technol 1990;24:679–92.
[14] Lenz J, Schurz J, Wrentschur E. Acta Polym 1992;43:307–12.
[15] Lenz J, Schurz J, Wrentschur E. Colloid Polym Sci 1992;271:460–8.
[16] Schurz J, Lenz J. Macromol Symp 1994;83:273–89.
[17] Blachot J-F, Dupeyre D, Verdier C. J Mater Sci 2001;36:4223–30.
[18] Smole MS, Peršin Z, Kreže T, Kleinschek KS, Ribitsch V, Neumayer S. Mater Res Innovations 2003;7:275–82.
[19] Batchelder DN, Bloor D. J Polym Sci: Polym Phys Ed 1979;17: 569–81.
[20] Young RJ. J Text Inst 1995;86:360–81.
[21] Hamad WY, Eichhorn SJ. ASME J Eng Mater Technol 1997;119: 309–13.
[22] Eichhorn SJ, Young RJ, Yeh WY. Text Res J 2001;71:121–9.
[23] Eichhorn SJ, Sirichaisit J, Young RJ. J Mater Sci 2001;36:3129–35.
[24] Eichhorn SJ, Young RJ, Davies GR. Biomacromolecules 2005;6: 507–13.
[25] Morton WE, Hearle JWS. Physical properties of textile fibres. Manchester: Textile Institute; 1993.
[26] Gedde UW. Polymer physics. London: Chapman and Hall; 1995.
[27] Bower DI, Maddams WF. The vibrational spectroscopy of polymers. Cambridge: Cambridge University Press; 1992.
[28] Hermans PH. Physics and chemistry of cellulose fibres. London: Elsevier Publishing Company; 1949.
[29] Marquardt DW. J Soc Ind Appl Math 1963;11:431.
[30] Mortimer SA, Péguy AA. Cell Chem Technol 1996;30:117–32.
[31] Atalla RH, Nagel SC. Science 1974;185:522–3.
[32] Wiley JH, Atalla RH. Carbohydr Res 1987;160:113–29.
[33] Edwards HGM, Farwell DW, Webster D. Spectrochim Acta Part A 1997;53:2383–92.
[34] Northolt MG. Polymer 1980;21:1199–204.
[35] Northolt MG, van der Hout R. Polymer 1985;6:310–6.
[36] Northolt MG, deVries H. Die Angew Makromol Chem 1985;133: 183–203.
[37] Bingham BEM. Makromol Chem 1964;77:139–52.
[38] Moss CE, Butler MF, Muller M, Cameron RE. J Appl Polym Sci 2001;83:2799–816.
[39] Langan P, Nishiyama Y, Chanzy H. J Am Chem Soc 1999;121: 9940–6.
[40] Langan P, Nishiyama Y, Chanzy H. Biomacromolecules 2001;2: 410–6.
[41] Šturcová A, His I, Wess TJ, Cameron G, Jarvis MC. Biomacromolecules 2003;4:1589–95.
[42] Kroon-Batenburg LMJ, Kroon J, Northolt MG. Polym Commun 1986; 27:290–2.
[43] Colom X, Carrillo F. Eur Polym J 2002;38:2225–30.
[44] Takayanagi M, Imada K, Kajiyama T. J Polym Sci C 1966;15:263.
[45] Ward IM. Mechanical properties of solid polymers. 2nd ed. New York: Wiley; 1985.
[46] Yeh W-Y, Young RJ. Polymer 1999;40:857–70.